Control of two-dimensional electronic states at anatase TiO_2 (001) surface by K adsorption

R. Yukawa,[1] M. Minohara,[1] D. Shiga,[1,2] M. Kitamura,[1] T. Mitsuhashi,[1,2] M. Kobayashi,[1] K. Horiba,[1] and H. Kumigashira[1,2,*]

[1]*Photon Factory, Institute of Materials Structure Science, High Energy Accelerator Research Organization (KEK), 1-1 Oho, Tsukuba 305-0801, Japan*

[2]*Department of Physics, Tohoku University, Sendai 980-8578, Japan*

(Received 18 January 2018; revised manuscript received 27 March 2018; published 23 April 2018)

The nature of the intriguing metallic electronic structures appearing at the surface of anatase titanium dioxide (a-TiO_2) remains to be elucidated, mainly owing to the difficulty of controlling the depth distribution of the oxygen vacancies generated by photoirradiation. In this study, K atoms were adsorbed onto the (001) surface of a-TiO_2 to dope electrons into the a-TiO_2 and to confine the electrons in the surface region. The success of the electron doping and its controllability were confirmed by performing *in situ* angle-resolved photoemission spectroscopy as well as core-level measurements. Clear subband structures were observed in the surface metallic states, indicating the creation of quasi-two-dimensional electron liquid (q2DEL) states in a controllable fashion. With increasing electron doping (K adsorption), the q2DEL states exhibited crossover from polaronic liquid states with multiple phonon-loss structures originating from the long-range Fröhlich interaction to "weakly correlated metallic" states. In the q2DEL states in the weakly correlated metallic region, a kink due to short-range electron–phonon coupling was clearly observed at about 80 ± 10 meV. The characteristic energy is smaller than that previously observed for the metallic states of a-TiO_2 with three-dimensional nature (∼110 meV). These results suggest that the dominant electron–phonon coupling is modulated by anisotropic carrier screening in the q2DEL states.

DOI: 10.1103/PhysRevB.97.165428

I. INTRODUCTION

Quasi-two-dimensional electron liquid (q2DEL) states formed at the surfaces of oxide semiconductors have exhibited remarkable phenomena such as universal subband structures irrespective of doping level [1], orbital-selective quantization [1–4], and possible giant spin splitting [5]. Knowledge about q2DEL states has great importance for understanding fundamental low-dimensional physics, as well as for designing future quantum electronic devices. Recently, metallic states formed at the (001) surface of anatase titanium dioxide (a-TiO_2) by irradiation with high-brilliance vacuum ultraviolet (VUV) light have been intensively studied using angle-resolved photoemission spectroscopy (ARPES) [6–8]. However, the behavior of the observed metallic states seems to differ between experiments, although the creation of metallic states by the photoirradiation itself is the same, which seems to be a common phenomenon for oxide–semiconductor surfaces [1–9]. For example, Moser *et al.* reported that metallic states were formed at the surface of a-TiO_2 and exhibited crossover from polaronic to "weakly correlated metallic" states with increasing irradiation time (carrier concentration) [6]. In addition, they claimed that the metallic states had three-dimensional (3D) character based on the normal emission ARPES results, where significant dispersion along the surface normal direction was observed. On the other hand, Rödel *et al.* and Wang *et al.* observed clear subband structures for the metallic states, indicating two-dimensional (2D) confinement of doped carriers, and asserted the 2D nature of the metallic states [7,8].

The controversy regarding the dimensionality of the metallic states may originate from differences between the depth distributions of the doped electrons, since it is difficult to control the depth distribution of the oxygen vacancies that act as electron donors by photoirradiation. In fact, the coexistence of 2D and 3D natures in metallic states has also been proposed to occur on other oxide semiconductors [10,11]. Thus, to elucidate the nature of the metallic states formed at an a-TiO_2 surface, especially whether or not the crossover from polaronic to weakly correlated metallic states is intrinsically linked to 3D nature, investigation using well-defined quantum-well structures is highly desired.

In this study, we performed electron doping onto an a-TiO_2 surface via *in situ* deposition of K atoms, where the K atoms were chemically adsorbed at the a-TiO_2 surface and doped electrons into the surface region [12], and investigated the evolution of the electronic structures by conducting *in situ* ARPES measurements. Using the relatively wide spot size of the synchrotron light at the Photon Factory, KEK, the influence of oxygen vacancies due to irradiation of light was virtually eliminated [13], although the metallic surface states derived from the oxygen vacancies in the topmost surface generated during growth remained. K atom deposition onto an a-TiO_2 surface causes the Fermi surface (FS) volume to evolve as a function of the amount of K adsorption. In this metallic state, clear subband structures have been observed, indicating that the doped electrons are confined in the surface region of a-TiO_2, which extends to a depth of a few nanometers. The q2DEL states exhibit crossover from polaronic states with multiple phonon-loss structures to weakly correlated metallic states

*Corresponding author: hiroshi.kumigashira@kek.jp

with a weak kink structure at 80 ± 10 meV with increasing electron doping (K adsorption). The characteristic energy of the kink is smaller than that of ~110 meV previously observed for metallic states of a-TiO_2 with 3D nature [6]. This result suggests that the dominant electron–phonon (e-p) coupling is modulated by anisotropic carrier screening in the q2DEL states.

II. EXPERIMENT

To prepare the samples, oxide-film growth was performed in a pulsed laser deposition (PLD) chamber and K deposition was subsequently conducted in a preparation chamber. These chambers were connected to a synchrotron-radiation photoemission spectroscopy system at undulator beam line BL-2A MUSASHI of the Photon Factory, KEK [14]. A-TiO_2 (001) films with a thickness of approximately 50 nm were epitaxially grown on $LaAlO_3$ (001) substrates via PLD [15]. To eliminate the charging effects in the ARPES measurements at low temperatures, a 0.2 at% Nb-doped TiO_2 pellet was used as the target. During a-TiO_2 deposition, the substrate temperature was held at 900 °C and the oxygen pressure was maintained at 1×10^{-5} Torr. The samples were subsequently annealed at 500 °C for 1 h under 10 Torr of oxygen and cooled to room temperature. Generally, post-annealing at a higher oxygen pressure is necessary to fill the oxygen vacancies that naturally form during growth. However, annealing at a higher oxygen pressure induces a significant increase in surface roughness and degradation of the microscopic crystalline quality of a-TiO_2 [16]. Therefore, we carefully optimized the post-annealing conditions and eventually adopted the modest oxygen pressure mentioned above, although residual carriers due to the oxygen vacancies in the topmost surface were not completely eliminated and a small resulting FS was observed in the ARPES data even with a bare a-TiO_2 surface. The q2DEL states derived from the topmost oxygen vacancies are described in detail later.

After the oxide films had been grown, K atoms were deposited onto them using a K dispenser. The K deposition rate was monitored by a quartz microbalance as well as by analyzing the relative intensities of the relevant core levels. As discussed in detail later, K atoms are randomly adsorbed onto the a-TiO_2 surface. Thus, we define the coverage of K atoms as the nominal thickness of the adsorbed K atoms obtained by assuming that the K-atoms accumulate onto the a-TiO_2 surface in the form of a body-centered cubic structure of K metal. The surface morphologies of the measured films were analyzed by performing *ex situ* atomic force microscopy in air. The crystal structures of the a-TiO_2 films were characterized via four-circle x-ray diffraction, which confirmed the epitaxial growth of the oxide films on the substrates.

In situ ARPES measurements were performed at 20 K using the linear vertical polarization of the synchrotron VUV light, while x-ray photoemission spectroscopy (XPS) measurements were conducted using the linear horizontal polarization of soft x-rays (see the Supplemental Material [17]: Fig. S1). The energy and angular resolutions were set to about 30 meV and 0.3°, respectively, for the ARPES measurements. For the XPS measurements, the total energy resolution was 150 meV at a photon energy of 800 eV. The Fermi level (E_F) of each sample was determined by measuring a gold film that was electrically connected to it. To prevent the oxidation of the deposited K atoms and avoid the resulting appearance of spurious peaks in the spectra, the oxide-film growth, K deposition, and subsequent spectroscopic measurements were performed *in situ*.

III. RESULTS AND DISCUSSION

A. Surface characterization

Before discussing the ARPES results, we provide evidence of the fact that irradiation with synchrotron light with a relatively wide spot size (200×500 μm^2) hardly induces evolution of the metallic states at the surfaces of a-TiO_2 films and that charge transfer from the adsorbed K atoms to the a-TiO_2 surface occurs. Figure 1 presents the results of surface characterization of bare a-TiO_2 and K/a-TiO_2. As can be seen from the temporal evolution of the Ti-2p core level obtained using bare a-TiO_2 [Fig. 1(a)], there are no detectable differences between before and after 15 min of synchrotron light irradiation: the Ti-2p core-level spectra clearly show Ti^{4+} states and do not show any indications of Ti^{3+} states. Since certain slight changes were observed in the spectra after 2 h of irradiation, we changed the location of the light spot on each sample every 15 min during the spectroscopic measurements.

The K deposition onto the (001) surface of a-TiO_2 causes a weak but distinct structure corresponding to Ti^{3+} states to appear at a binding energy of 457.5 eV, as shown in Fig. 1(b), indicating that electrons are transferred from the K atoms to the a-TiO_2 films and that the doped electrons accumulate near the surface region accessible by the present XPS measurements [~1 nm away from the a-TiO_2 surface (the interface between K and a-TiO_2)] [21]. With further increasing the amount of K deposition, the Ti^{3+} states exhibit systematic evolution, which seems to saturate above 0.8 Å. These results imply that a certain amount of electron doping is induced by K deposition. The evolution of the Ti^{3+} states as a function of K deposition is summarized in Fig. 1(c) [22]. We deconvoluted the Ti-2$p_{3/2}$ core levels using two Voigt functions with a smooth Shirley background to determine the contributions of the Ti^{4+} and Ti^{3+} states. The occurrence of electron doping is also confirmed by the shift of the Ti^{4+} peak by ~190 meV due to band bending, although the actual band bending might be larger owing to residual carriers from the oxygen vacancies at the bare surface. It should be noted that similar saturation behaviors of the Ti^{3+} states and band bending were observed in the case of photoirradiation [7].

The next crucial issue is the chemical states of the K atoms on the surfaces of the a-TiO_2 films. When the K/a-TiO_2 samples were heated to 650 °C in ultra-high vacuum conditions, the K signals in the XPS spectra nearly disappear, as do the Ti^{3+} states almost simultaneously, as shown in the top panel of Fig. 1(b). Moreover, the Ti^{4+} peak returns to its position in the case of the bare surface, indicating that the band bending induced by K deposition is entirely removed. Figure 1(d) shows the low-energy electron diffraction (LEED) patterns before K deposition (bare a-TiO_2 surface), after K deposition, and after subsequent heat treatment for thermal desorption of the K atoms. Sharp 1×1 spots with surface-reconstruction-derived

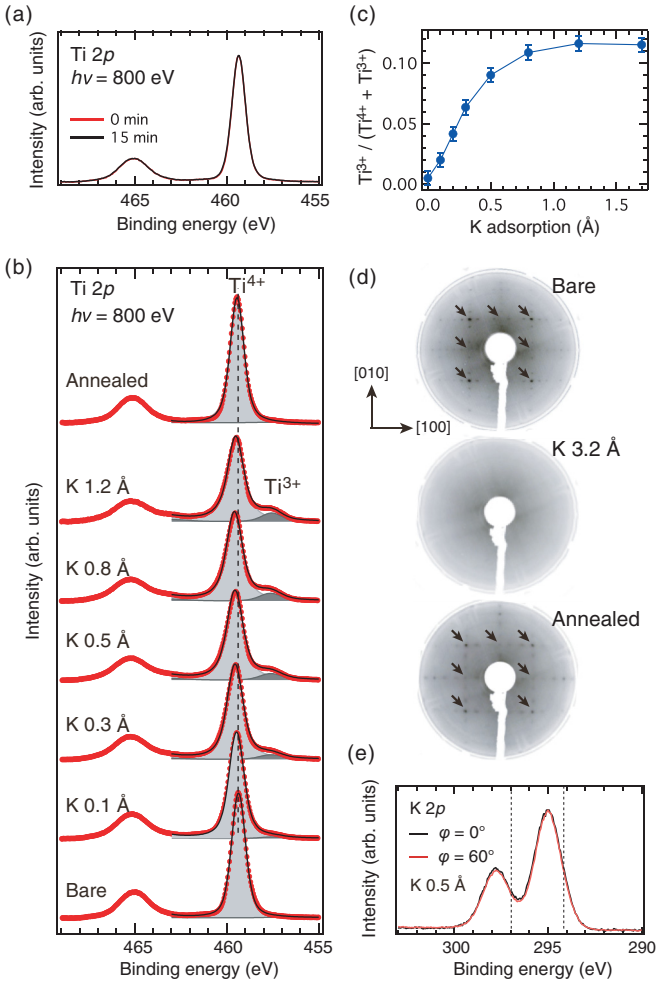

FIG. 1. (a) Ti-2p core-level spectra corresponding to the bare a-TiO_2 (001) surface shortly after the first photoirradiation (red) and after 15 min of light irradiation (black). (b) Ti-2p core-level spectra of a-TiO_2 obtained by varying the coverage of adsorbed K atoms. The curve fitting results for the Ti-2$p_{3/2}$ states are presented, where the components of the Ti^{4+} and Ti^{3+} states are indicated by different hatching. The dashed line indicates the peak position of the Ti-2$p_{3/2}$ states for a bare a-TiO_2 (001) surface. All of the XPS spectra shown in (a) and (b) are taken in the normal emission (polar angle $\varphi = 0^\circ$) geometry. (c) The plot of relative intensities of the Ti^{3+} states as a function of adsorbed K. (d) LEED patterns of a-TiO_2 surfaces before K deposition (bare surface), after 3.2 Å K deposition, and after subsequent heat treatment for thermal desorption of K. The 1 × 1 spots with surface-reconstruction-derived 1 × 4 spots are clearly observed for the bare and reannealed surfaces. The arrows indicate the 1 × 1 spots. (e) Angular dependence of K-2p core-level spectra taken for the K/a-TiO_2 with 0.5 Å K deposition. The dotted lines indicate the chemical shift of K metal [17].

1 × 4 spots are observed at the bare surface [23], reflecting the high crystallinity of the film surface. K deposition causes these sharp spots to be completely smeared out, suggesting that the K atoms are randomly adsorbed onto the a-TiO_2 surface. The original sharp LEED pattern of the bare surface is recovered by annealing. The absence of any changes in the LEED patterns between the bare a-TiO_2 surface and the surface after re-evaporation of the K atoms suggests their adsorbing nature. The adsorbing nature is further supported by the K-2p core-level measurements [Fig. 1(e)]. The absence of any detectable angular dependence of the K-2p core level implies that the K atoms stick to the surface and do not diffuse into the a-TiO_2. A closer look at the core-level line shape reveals that the K-2$p_{3/2}$ peak is located at a binding energy of 295.0 eV, which is different from those of both K metals (294.7 eV) [24] and K oxides (292.3–292.9 eV) [25–27], and the peak width is much wider than that of K metal (see the Supplemental Material [17]: Fig. S2). These features of the K-2p core level are quite similar to those of a disperse adsorbate phase of K atoms on a metal surface [28–33], suggesting that K atoms are chemically adsorbed on a-TiO_2 surfaces and provide the Ti-3d states with electrons, as in the case of K adsorption on rutile TiO_2 surfaces [34–36].

B. ARPES results

The increment of the sheet carrier density (n_{2D}) associated with K deposition has been clearly observed in the *in situ* ARPES measurements. Figure 2(a) shows a series of ARPES images taken along the [100] direction as a function of K adsorption. Clear subband structures are observed in all of the ARPES images for the K-adsorbed surfaces, indicating the 2D nature of the observed conduction bands (see the Supplemental Material [17]: Fig. S3). As described above, the metallic states due to residual oxygen vacancies in the topmost surface exist even for a bare a-TiO_2 surface. The 2D nature of the metallic states at a bare a-TiO_2 surface is also supported by the existence of subband structures (see the Supplemental Material [17]: Fig. S3). This is sharp contrast to the 3D nature of metallic states created by photoirradiation, where the oxygen vacancies are distributed in depth, suggesting that the oxygen vacancies in the topmost surface also act as electron donors, like adsorbed K atoms. By deposition of K atoms onto the a-TiO_2 surface, the Fermi momentum (k_F) determined from momentum distribution curves (MDCs) increases from 0.11 $Å^{-1}$ for the bare a-TiO_2 film to 0.19 $Å^{-1}$ for the a-TiO_2 film with 0.5 Å K adsorption. Because a-TiO_2 forms a Ti-3d-t_{2g} d_{xy}-derived circular FS centered at the $\bar{\Gamma}$ point [Fig. 2(b)], the increase in k_F may reflect the increase in n_{2D} by K deposition [8]. The n_{2D} values obtained from the Luttinger volumes based on the assumption of spin degeneracy of the subbands are plotted in Fig. 2(c) as a function of K deposition. The n_{2D} value steeply increases with increasing K deposition and seems to saturate at 0.3 Å.

The dependence of n_{2D} on the K-deposition seems to differ from that of Ti^{3+} states [see Fig. 1(c)]. In contrast to the saturation of n_{2D} at 0.3 Å K deposition, the intensity of Ti^{3+} states continues to increase after 0.3 Å K deposition and seems to saturate at about 0.8 Å. Assuming that the Ti^{3+} states observed in the Ti-2p core levels reflect the contributions of both localized and mobile electrons (namely, activated carriers whose density corresponds to n_{2D}) [37], these results suggest the charges transferred from K atoms to a-TiO_2 are partially trapped in the surface region. It should be noted that the existence of localized electrons at the interface between the a-TiO_2 and adsorbed K atoms is further supported by the angular

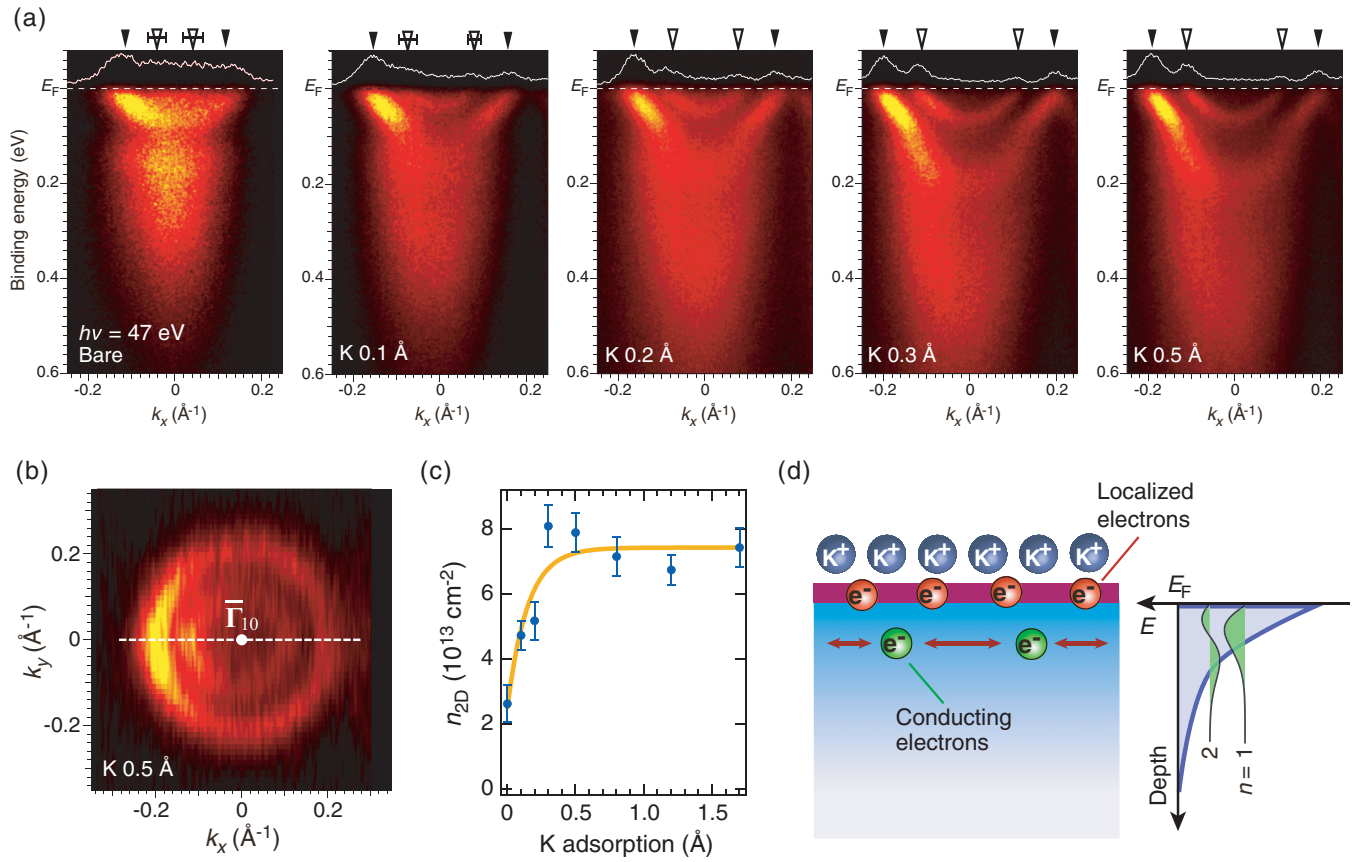

FIG. 2. (a) ARPES images taken at $h\nu = 47$ eV for K-adsorbed surfaces of a-TiO_2 with varying K coverage. The ARPES spectra were measured along the k_x direction across the $\bar{\Gamma}_{10}$ point [dashed line in (b)]. The MDCs at E_F with an energy window of 10 meV are also shown in the respective images. (b) FS mapping around the $\bar{\Gamma}_{10}$ point for K 0.5 Å. The two concentric circular FSs originating from subband formation are clearly observed. (c) The plot of n_{2D} estimated from ARPES measurements as a function of K coverage. (d) Schematic illustration of the possible structure model explaining the charge transfer from adsorbed K atoms to an a-TiO_2 surface and the resulting accumulation-layer formation.

dependence of the Ti-2p states (see the Supplemental Material [17]: Fig. S4).

The possible structure model explaining charge transfer from adsorbed K atoms to an a-TiO_2 surface and the resulting accumulation-layer formation is drawn in Fig. 2(d). Since the ionic radius of a K atom is sufficiently large that adsorbed K atoms do not diffuse into a-TiO_2 [38], the K atoms stick to the topmost surface of a-TiO_2 and provide the a-TiO_2 with electrons. Some of the transferred electrons may be preferentially accumulated in the surface regions initially. The analysis of the observed quantized states with a triangular wedge potential suggests that the activated carriers contributing to the formation of q2DEL states are confined in the surface (interface) region extending to a depth of a few nanometers. Meanwhile, the excess electrons could be trapped around K ions and/or oxygen vacancies at the interface between the K and a-TiO_2. The two kinds of behavior of the transferred electrons probably explain the saturation of n_{2D} at lower K adsorption. Note that similar saturation behaviors of Ti^{3+} states and n_{2D} have been observed in the case of photoirradiation [7]. This picture is consistent with the recent theoretical calculations related to oxygen vacancies in oxide semiconductors, where excess electrons do not fill up the conduction band, but rather form only localized states [39]. To clarify the mechanism for the different behaviors of transferred electrons, further investigations of the detailed surface and interface structures and their relations to the carrier concentration of a-TiO_2 are required.

We now turn our attention to the evolution of the ARPES spectral shape associated with the increase in n_{2D} (K deposition). As can be seen in Fig. 2(a), the ARPES images exhibit systematic changes reminiscent of the crossover from polaronic to Fermi liquid states via weakly correlated metallic states in $SrTiO_3$ (001) surfaces [40]. The ARPES image for the bare a-TiO_2 surface depicts the typical behavior of polaronic liquid states: parabolic bands near E_F concomitant with satellite replica structures with energy intervals of 100–150 meV below a binding energy of 100 meV. As discussed in detail later, these intensities are well described by the Franck–Condon model, where electrons in metallic states lose their energy by exciting phonons [6,40,41]. Based on this analysis, the parabolic bands in the binding energy of $E_F - 100$ meV assigned to the quasiparticle (QP) bands. In addition, a closer look revealed the existence of relatively weak but distinct structures inside the parabolic band [17]. The outer and inner bands are assigned to the first ($n = 1$) and second ($n = 2$)

subbands, respectively, indicating that the polaronic liquid state is also realized in the q2DEL states of a-TiO_2.

Upon K adsorption, the metallic states evolve from polaronic to weakly correlated metallic states. With increasing K deposition, the satellite structures distributed below ~100 meV become weak, while the QP states in the vicinity of E_F become prominent [17]. As a result, the subband structures are more clearly visible for the K-adsorbed surface. Simultaneously, the n_{2D} increases from $2.3 \pm 0.5 \times 10^{13}$ cm^{-2} for the bare surface to $7.4 \pm 0.6 \times 10^{13}$ cm^{-2} on average for the surfaces with $K > 0.3$ Å, suggesting that the doped mobile electrons are also accommodated in the q2DEL states in the surface region. Furthermore, a kink in the band dispersion emerges near E_F. These changes in the ARPES images indicate the occurrence of the crossover from polaronic liquid states with multiple phonon-loss structures to weakly correlated metallic states with short-range e-p coupling by increasing n_{2D}. These results suggest that the crossover of q2DEL as a function of carrier concentration is common feature in oxide semiconductors [42].

To investigate the crossover in more detail, we have performed line shape analysis of the ARPES spectra. For this analysis, we have utilized the ARPES data taken at $h\nu = 83$ eV with the other conditions remaining the same, where the intensity of the $n = 1$ subband is prominent and consequently the contributions of the other subbands ($n \geqslant 2$) are negligible, as shown in Fig. 3(a). It should be noted that although the relative intensities of the subbands strongly change with $h\nu$, the subband dispersions themselves remain unchanged owing to the 2D character of the quantized states [43] (see the Supplemental Material [17]: Fig. S6). Conversely, the observed strong $h\nu$ dependence provides further evidence of the quantized (2D) nature of the electronic structure observed near E_F.

The spectral changes with increasing carrier concentration are clearly visible in the ARPES spectra at k_F, as shown in Fig. 3(b). The "peak-dip-hump" structure characteristic to the polaronic liquid system [6,40] is clearly observed for the bare surface. To evaluate the energy scale, the ARPES spectra are fitted using the Franck-Condon model with a single phonon mode. In the fitting, the QP peak at E_F is represented by a Lorentzian and its satellites (multiple phonon-loss structures) by Gaussians with an energy interval of 150 meV [6]. The peak integrals are restricted to follow the Poisson distribution [44]. This characteristic energy scale agrees well with the previous results for 3D metallic states formed at the surface of a-TiO_2 by photoirradiation [6] and is close to the excitation energy of the longitudinal-optical (LO) E_u phonon (108 meV) [45]. Therefore, the satellite peaks most probably originate from the long-range Fröhlich interaction between the confined electrons and LO phonons of a-TiO_2 [6,42]. These line-shape analyses reveal that the q2DEL states of the bare surface could be regarded as a polaronic liquid where the confined electrons strongly interact with the LO phonons [6]. On the other hand, with increasing K deposition onto the a-TiO_2 surface, the peak–dip–hump structures gradually smear out and are no longer resolved above 0.2 Å K deposition, indicating the breakdown of the polaronic liquid at higher carrier densities [6].

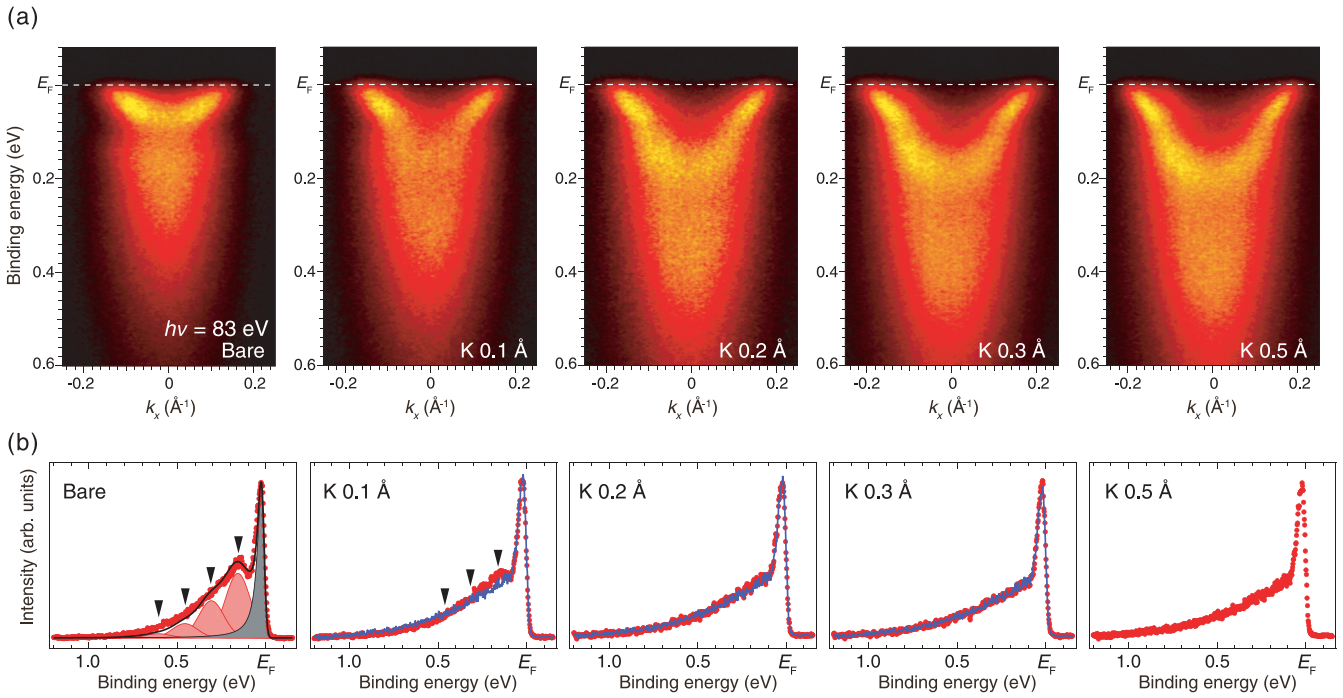

FIG. 3. (a) ARPES images taken at $h\nu = 83$ eV with the other conditions remaining the same as those used to obtain Fig. 2(a) for a K-adsorbed a-TiO_2 surface with varying K coverage. (b) Respective EDCs at k_F after subtracting the momentum-independent background [17]. The characteristic peak–dip–hump structure is observed for the bare surface and seems to smear out with increasing K deposition (carrier concentration). For the bare a-TiO_2 surface, the fitting results based on the Franck–Condon model are superimposed. The EDC of 0.5 Å K adsorption (solid blue curve) is overlaid with those of 0.1−0.3 Å adsorption to highlight the spectral evolution associated with the crossover.

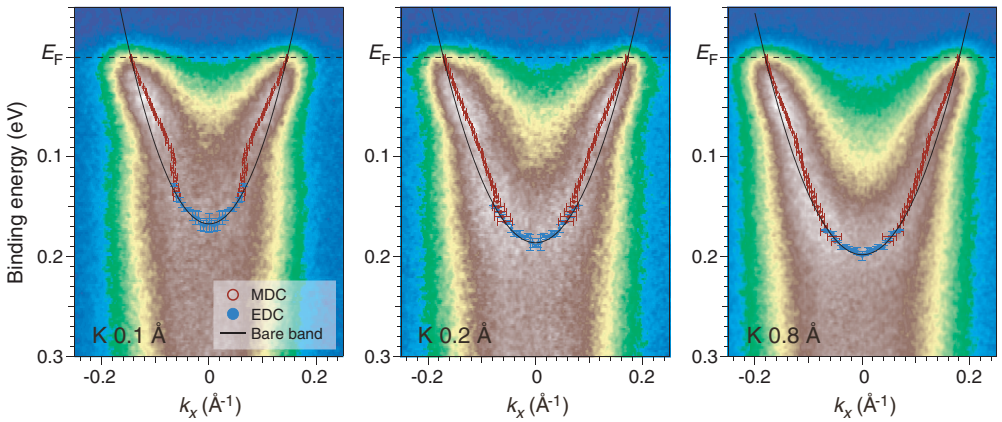

FIG. 4. ARPES intensity plots taken at $h\nu = 83$ eV for K coverages of 0.1 Å, 0.2 Å, and 0.8 Å. The peak positions of the MDCs and EDCs are indicated by open red and filled blue circles, respectively. These peak positions were determined by fitting the MDCs and EDCs to the linear combination of Lorentzians and a smooth background. The results of band-structure calculation in the renormalized-band scheme are also overlaid as a bare band.

According to a recent theoretical study by Verdi *et al.*, the e-p interactions for LO phonons are well screened by doped carriers when the plasma frequency of the carriers exceeds the frequency of the LO phonon mode [42]. Based on this model, the critical carrier density at which crossover from the polaronic regime to the Fermi liquid regime starts to evolve can be roughly estimated to be $\sim 1.4 \times 10^{13}$ cm^{-2} for the q2DEL states of a-TiO_2 assuming electron confinement in a few-nanometer-thick surface region of bulk a-TiO_2 [42]. Based on the spectral evolution as a function of n_{2D} (K adsorption) in Fig. 3(b), the critical carrier density of the q2DEL states of a-TiO_2 is estimated to be $3.9-5.5 \times 10^{13}$ cm^{-2} (K adsorption of 0.1−0.2 Å). The good agreement between the experimental and theoretical critical carrier densities suggests that the interaction between the electrons and LO phonons is also important in the q2DEL states at the surface of a-TiO_2. It should be noted that similar saturation behavior at the critical n_{2D} has also been observed in q2DEL states at a photo-irradiated $SrTiO_3$ (001) surface [40].

In contrast to the reduction of the polaronic satellites, the kink structures in the QP dispersion near E_F become visible in the weakly correlated metallic region. Figure 4 displays the band dispersions of 0.1 Å, 0.2 Å, and 0.8 Å K/a-TiO_2 that are obtained from the plot of the peak positions of the MDCs and energy distribution curves (EDCs). The results of band-structure calculations in the renormalized-band scheme [46,47] are also overlaid for all of the band dispersions as a bare band (see the Supplemental Material [17]: Fig. S8). In comparison with the bare band, a clear kink at a characteristic energy of 80 ± 10 meV is clearly visible in the band dispersion in each ARPES image. Furthermore, the kink structure becomes weak with increasing n_{2D}. From the observed kink, the coupling constant $\lambda_{e\text{-}p}$ due to the short-range e-p interaction is evaluated using $\lambda_{e\text{-}p} = (v_b/v_F - 1)$, where v_b and v_F are the Fermi velocities of the bare and experimentally observed bands, respectively. $\lambda_{e\text{-}p}$ are estimated to be 0.83 ± 0.04, 0.59 ± 0.04, and 0.44 ± 0.04 for 0.1 Å, 0.2 Å, and 0.8 Å K deposition, respectively. The decrease of $\lambda_{e\text{-}p}$ with increasing n_{2D} may reflect increased screening of the short-range e-p coupling, as well as the long-range coupling, by conduction electrons [6,40,42].

Finally, we discuss the characteristic energy of the observed kink in q2DEL states of a-TiO_2. The kink energy of 80 ± 10 meV is smaller than that corresponding to the metallic states of a-TiO_2 with 3D character [6,42]. Moser *et al.* reported the existence of a kink structure at ∼110 meV in metallic states of a-TiO_2 with 3D character [6], and the subsequent theoretical study of bulk a-TiO_2 demonstrated that the coupling to LO E_u phonons (∼ 108 meV) predominately contributes to this kink structure [42]. Although the origin of the difference between bulk a-TiO_2 and q2DEL states is not clear at the moment, one possible explanation is the modulation of the e-p coupling to E_u phonons by anisotropic carrier screening in the q2DEL states. In the q2DEL states, the electrons confined within a few nanometers from the surface contribute to the screening of the e-p coupling. In this situation, the 2D screening might be expected to suppress the e-p coupling to in-plane E_u phonons [42,45]; consequently, the e-p coupling with other phonon excitations predominantly contributes to the kink formation. Further investigations are required to clarify the origin of reduction of the kink energy in q2DEL states; in particular, more accurate calculations will be necessary to account for the 2D screening in q2DEL states.

IV. CONCLUSION

We performed *in situ* ARPES studies of the q2DEL states formed on a-TiO_2 (001) surfaces. To control the q2DEL states, K atoms were chemically adsorbed onto the surfaces to dope electrons into the a-TiO_2 and confine them in the surface regions. The success of the electron doping and its controllability were confirmed by conducting *in situ* ARPES as well as core-level measurements. Clear subband structures were observed for the surface metallic states, indicating the creation of q2DEL states in a controllable fashion. With increasing electron doping (K adsorption), the q2DEL states exhibited crossover from polaronic liquid states with multiple phonon-loss structures originating from the long-range Fröhlich interaction to weakly

correlated metallic states with a kink caused by short-range e-p coupling, suggesting that the crossover of q2DEL states with increasing carrier concentration is a common feature of oxide semiconductors. In the weakly correlated metallic states, a kink was observed at about 80 ± 10 meV, and it became weak with increasing carrier concentration, reflecting the screening of the e-p coupling by conduction electrons. The characteristic energy of the kink in q2DEL states is less than that previously observed for the metallic states of a-TiO_2 with 3D nature. These results suggest that the e-p coupling reflects anisotropic carrier screening in q2DEL states.

ACKNOWLEDGMENTS

The authors are very grateful to A. Santander-Syro, K. Ozawa, and Y. Kuramoto for the useful discussions. This work was financially supported by Grants-in-Aid for Scientific Research (No. 16H02115, No. 16KK0107, and No. 17K14325) from the Japan Society for the Promotion of Science (JSPS) and the MEXT Elements Strategy Initiative to Form Core Research Center. This work at KEK-PF was performed under the approval of the Program Advisory Committee (Proposals No. 2015S2005 and No. 2016G164) at the Institute of Materials Structure Science at KEK.

[1] A. F. Santander-Syro, O. Copie, T. Kondo, F. Fortuna, S. Pailhès, R. Weht, X. G. Qiu, F. Bertran, A. Nicolaou, A. Taleb-Ibrahimi, P. Le Fèvre, G. Herranz, M. Bibes, N. Reyren, Y. Apertet, P. Lecoeur, A. Barthélémy, and M. J. Rozenberg, Nature **469**, 189 (2011).

[2] A. F. Santander-Syro, C. Bareille, F. Fortuna, O. Copie, M. Gabay, F. Bertran, A. Taleb-Ibrahimi, P. Le Fèvre, G. Herranz, N. Reyren, M. Bibes, A. Barthélémy, P. Lecoeur, J. Guevara, and M. J. Rozenberg, Phys. Rev. B **86**, 121107(R) (2012).

[3] T. C. Rödel, C. Bareille, F. Fortuna, C. Baumier, F. Bertran, P. Le Fèvre, M. Gabay, O. Hijano Cubelos, M. J. Rozenberg, T. Maroutian, P. Lecoeur, and A. F. Santander-Syro, Phys. Rev. Appl. **1**, 051002 (2014).

[4] P. D. C. King, S. McKeown Walker, A. Tamai, A. de la Torre, T. Eknapakul, P. Buaphet, S.-K. Mo, W. Meevasana, M. S. Bahramy, and F. Baumberger, Nat. Commun. **5**, 3414 (2014).

[5] A. F. Santander-Syro, F. Fortuna, C. Bareille, T. C. Rödel, G. Landolt, N. C. Plumb, J. H. Dil, and M. Radović, Nat. Mater. **13**, 1085 (2014)

[6] S. Moser, L. Moreschini, J. Jaćimović, O. S. Barišić, H. Berger, A. Magrez, Y. J. Chang, K. S. Kim, A. Bostwick, E. Rotenberg, L. Forró, and M. Grioni, Phys. Rev. Lett. **110**, 196403 (2013).

[7] T. C. Rödel, F. Fortuna, F. Bertran, M. Gabay, M. J. Rozenberg, A. F. Santander-Syro, and P. Le Fèvre, Phys. Rev. B **92**, 041106(R) (2015).

[8] Z. Wang, Z. Zhong, S. McKeown Walker, Z. Ristic, J.-Z. Ma, F. Y. Bruno, S. Riccò, G. Sangiovanni, G. Eres, N. C. Plumb, L. Patthey, M. Shi, J. Mesot, F. Baumberger, and M. Radovic, Nano Lett. **17**, 2561 (2017).

[9] W. Meevasana, P. D. C. King, R. H. He, S.-K. Mo, M. Hashimoto, A. Tamai, P. Songsiriritthigul, F. Baumberger, and Z.-X. Shen, Nat. Mater. **10**, 114 (2011).

[10] S. Harashima, C. Bell, M. Kim, T. Yajima, Y. Hikita, and H. Y. Hwang, Phys. Rev. B **88**, 085102 (2013).

[11] N. C. Plumb, M. Salluzzo, E. Razzoli, M. Månsson, M. Falub, J. Krempasky, C. E. Matt, J. Chang, M. Schulte, J. Braun, H. Ebert, J. Minár, B. Delley, K.-J. Zhou, T. Schmitt, M. Shi, J. Mesot, L. Patthey, and M. Radović, Phys. Rev. Lett. **113**, 086801 (2014).

[12] Y. K. Kim, O. Krupin, J. D. Denlinger, A. Bostwick, E. Rotenberg, Q. Zhao, J. F. Mitchell, J. W. Allen, and B. J. Kim, Science **345**, 187 (2014).

[13] S. Backes, T. C. Rödel, F. Fortuna, E. Frantzeskakis, P. Le Fèvre, F. Bertran, M. Kobayashi, R. Yukawa, T. Mitsuhashi, M. Kitamura, K. Horiba, H. Kumigashira, R. Saint-Martin, A. Fouchet, B. Berini, Y. Dumont, A. J. Kim, F. Lechermann, H. O. Jeschke, M. J. Rozenberg, R. Valentí, and A. F. Santander-Syro, Phys. Rev. B **94**, 241110(R) (2016).

[14] K. Horiba, H. Ohguchi, H. Kumigashira, M. Oshima, K. Ono, N. Nakagawa, M. Lippmaa, M. Kawasaki, and H. Koinuma, Rev. Sci. Instrum. **74**, 3406 (2003).

[15] M. Murakami, Y. Matsumoto, K. Nakajima, T. Makino, Y. Segawa, T. Chikyow, P. Ahmet, M. Kawasaki, and H. Koinuma, Appl. Phys. Lett. **78**, 2664 (2001).

[16] M. Katayama, S. Ikesaka, J. Kuwano, H. Koinuma, and Y. Matsumoto, Appl. Phys. Lett. **92**, 132107 (2008).

[17] See Supplemental Material at http://link.aps.org/supplemental/10.1103/PhysRevB.97.165428 for the experimental geometry in the present ARPES measurements, the surface characterization of measured samples, and the analytical procedures of ARPES results, which includes Refs. [18–20].

[18] P. D. C. King, H. I. Wei, Y. F. Nie, M. Uchida, C. Adamo, S. Zhu, X. He, I. Božović, D. G. Schlom, and K. M. Shen, Nat. Nanotechnol. **9**, 443 (2014).

[19] T. Yoshida, K. Tanaka, H. Yagi, A. Ino, H. Eisaki, A. Fujimori, and Z.-X. Shen, Phys. Rev. Lett. **95**, 146404 (2005).

[20] B. J. Kim, H. Koh, E. Rotenberg, S.-J. Oh, H. Eisaki, N. Motoyama, S. Uchida, T. Tohyama, S. Maekawa, Z.-X. Shen, and C. Kim, Nat. Phys. **2**, 397 (2006).

[21] S. Tanuma, C. J. Powell, and D. R. Penn, Surf. Interface Anal. **43**, 689 (2011).

[22] It should be noted that the intensity ratios of $Ti^{3+}/(Ti^{4+} + Ti^{3+})$ shown in Fig. 1(c) are results of the photoelectron signals from Ti^{3+} and Ti^{4+} ions that differently distribute over the whole probing depth (∼1.0 nm in this present experimental conditions Ref. [21]) and hence do not straightforwardly correspond to the $Ti^{3+}/(Ti^{4+} + Ti^{3+})$ composition ratio at the surface Ref. [17].

[23] G. S. Herman and M. R. Sievers, Phys. Rev. Lett. **84**, 3354 (2000).

[24] L.-G. Petersson and S.-E. Karlsson, Phys. Scr. **16**, 425 (1977).

[25] J.-S. Kang, D. H. Kim, J. H. Hwang, J. Baik, H. J. Shin, M. Kim, Y. H. Jeong, and B. I. Min, Phys. Rev. B **82**, 193102 (2010).

[26] M. Oku, J. Electron Spectros. Relat. Phenomena **74**, 135 (1995).

[27] J. Kubacki, A. Molak, M. Rogala, C. Rodenbücher, and K. Szot, Surf. Sci. **606**, 1252 (2012).

[28] S. Modesti, C. T. Chen, Y. Ma, G. Meigs, P. Rudolf, and F. Sette, Phys. Rev. B **42**, 5381(R) (1990).

[29] Y.-M. Sun, H. S. Luftman, and J. M. White, Surf. Sci. **139**, 379 (1984).

[30] J. J. Weimer, E. Umbach, and D. Menzel, Surf. Sci. **159**, 83 (1985).
[31] G. Pirug, A. Winkler, and H. P. Bonzel, Surf. Sci. **163**, 153 (1985).
[32] T. Aruga, H. Tochihara, and Y. Murata, Surf. Sci. **175**, L725 (1986).
[33] Z. P. Hu, N. J. Wu, and A. Ignatiev, Phys. Rev. B **33**, 7683 (1986).
[34] R. Casonava, K. Prabhakaran, and G. Thornton, J. Phys. Condens. Matter **3**, S91 (1991).
[35] K. Prabhakaran, D. Purdie, R. Casanova, C. A. Muryn, P. J. Hardman, P. L. Wincott, and G. Thornton, Phys. Rev. B **45**, 6969(R) (1992).
[36] P. J. Hardman, R. Casanova, K. Prabhakaran, C. A. Muryn, P. L. Wincott, and G. Thornton, Surf. Sci. **269-270**, 677 (1992).
[37] A. Koitzsch, J. Ocker, M. Knupfer, M. C. Dekker, K. Dörr, B. Büchner, and P. Hoffmann, Phys. Rev. B **84**, 245121 (2011).
[38] R. D. Shannon, Acta Crystallogr. Sect. A **32**, 751 (1976).
[39] C. Di Valentin, G. Pacchioni, and A. Selloni, J. Phys. Chem. C **113**, 20543 (2009).
[40] Z. Wang, S. McKeown Walker, A. Tamai, Y. Wang, Z. Ristic, F. Y. Bruno, A. de la Torre, S. Riccò, N. C. Plumb, M. Shi, P. Hlawenka, J. Sánchez-Barriga, A. Varykhalov, T. K. Kim, M. Hoesch, P. D. C. King, W. Meevasana, U. Diebold, J. Mesot, B. Moritz, T. P. Devereaux, M. Radovic, and F. Baumberger, Nat. Mater. **15**, 835 (2016).
[41] R. Yukawa, K. Ozawa, S. Yamamoto, H. Iwasawa, K. Shimada, E. F. Schwier, K. Yoshimatsu, H. Kumigashira, H. Namatame, M. Taniguchi, and I. Matsuda, Phys. Rev. B **94**, 165313 (2016).
[42] C. Verdi, F. Caruso, and F. Giustino, Nat. Commun. **8**, 15769 (2017).
[43] M. Kobayashi, K. Yoshimatsu, E. Sakai, M. Kitamura, K. Horiba, A. Fujimori, and H. Kumigashira, Phys. Rev. Lett. **115**, 076801 (2015).
[44] G. D. Mahan, *Many-Particle Physics*, 3rd ed. (Kluwer Academic/Plenum Publishers, New York, 2000).
[45] R. J. Gonzalez, R. Zallen, and H. Berger, Phys. Rev. B **55**, 7014 (1997).
[46] K. Yoshimatsu, K. Horiba, H. Kumigashira, T. Yoshida, A. Fujimori, and M. Oshima, Science **333**, 319 (2011).
[47] T. Hitosugi, H. Kamisaka, K. Yamashita, H. Nogawa, Y. Furubayashi, S. Nakao, N. Yamada, A. Chikamatsu, H. Kumigashira, M. Oshima, Y. Hirose, T. Shimada, and T. Hasegawa, Appl. Phys. Express **1**, 111203 (2008).